

# Higgs-dilaton cosmology: An inflation – dark-energy connection and forecasts for future galaxy surveys

Santiago Casas, Martin Pauly, and Javier Rubio  
*Institut für Theoretische Physik,  
 Ruprecht-Karls-Universität Heidelberg,  
 Philosophenweg 16, 69120 Heidelberg, Germany*

The Higgs-Dilaton model is a scale-invariant extension of the Standard Model non-minimally coupled to gravity and containing just one additional degree of freedom on top of the Standard Model particle content. This minimalistic scenario predicts a set of measurable consistency relations between the inflationary observables and the dark-energy equation-of-state parameter. We present an alternative derivation of these consistency relations that highlights the connections and differences with the  $\alpha$ -attractor scenario. We study how far these constraints allow one to distinguish the Higgs-Dilaton model from  $\Lambda$ CDM and  $w$ CDM cosmologies. To this end we first analyze existing data sets using a Markov Chain Monte Carlo approach. Second, we perform forecasts for future galaxy surveys using a Fisher matrix approach, both for galaxy clustering and weak lensing probes. Assuming that the best fit values in the different models remain comparable to the present ones, we show that both Euclid- and SKA2-like missions will be able to discriminate a Higgs-Dilaton cosmology from  $\Lambda$ CDM and  $w$ CDM.

## I. INTRODUCTION

We are entering an era of precision cosmology in which many of the ingredients of our standard cosmological scenario will be tested with an unprecedented level of precision. By ruling out a vast set of models, future cosmological surveys such as DESI, Euclid or SKA will shed light on fundamental aspects of modern physics such as inflation and dark energy.

The interpretation of future cosmological observations is inevitably influenced by our initial set of assumptions. An example of this is the usual treatment of inflation and dark energy as two completely independent epochs in the history of the Universe. Note, however, that there is no fundamental reason for this to be the case. Inflation and dark energy indeed share many essential properties that could be related to some underlying principle able to unify them within a common framework. Among the different implementations of this idea proposed in the literature, the models based on scale and conformal symmetry are particularly interesting [1–15] since they could additionally alleviate the Standard Model hierarchy problem [16–18] (see also Refs. [19, 20]).

In this paper we will assume scale invariance to be an exact but spontaneously broken symmetry [17]. The simplest realization of this idea is the so-called Higgs-Dilaton (HD) scenario [5, 6]. This model is a minimalistic extension of the Standard Model (SM) based on dilatation symmetry and unimodular gravity. Both the Planck scale and the Higgs vacuum expectation value are replaced by a singlet scalar field  $\chi$ , which, together with the Higgs field  $H$ , is allowed to be non-minimally coupled to gravity. While the non-minimal couplings allow for inflation with the usual SM Higgs potential, the unimodular restriction allows to recover the late time acceleration of the Universe *even in the absence of a cosmological constant* in the action. The HD model is close to  $\Lambda$ CDM in terms of background evolution but contrary to this sce-

nario it connects the early and the late Universe in a very non-trivial way. In particular, it relates the existence of a dynamical dark energy component to deviations from the  $\alpha$ -attractor inflationary predictions [21–23]. This is a unique connection between two eras far apart in the evolution of the Universe that could be potentially tested with future cosmological surveys.

In this work we study the impact of the HD consistency relations on cosmological observables. The main ideas and phenomenology of the HD model are introduced in Section II, where we present a novel derivation of the HD consistency relations that highlights the connections and differences with the well-known  $\alpha$ -attractor scenario [21–23]. In Section III we use a Markov Chain Monte Carlo approach to analyze current data sets in the presence of the HD constraints. We discuss the chances of differentiating the HD model from other cosmological scenarios such as  $\Lambda$ CDM or  $w$ CDM. The impact of the consistency relations on the results of future cosmological observations is explored in Section IV via a Fisher matrix approach. Our reference surveys are a DESI-like [24, 25], a Euclid-like [26, 27] and a SKA2-like [28–31] galaxy survey measuring the expansion history of the Universe and the evolution of large scale structures up to a redshift  $z \sim 2$ . The conclusions of our analysis are presented in Section V.

## II. THE HIGGS-DILATON MODEL

The key ingredients of the HD model are scale-invariance (SI) and unimodular gravity (UG). In the unitary gauge  $H = (0, h/\sqrt{2})^T$ , the graviscalar sector of the HD Lagrangian density takes the form [5, 6]

$$\mathcal{L}_{SI+UG} = \frac{f(h, \chi)}{2} R - \frac{1}{2} (\partial h)^2 - \frac{1}{2} (\partial \chi)^2 - V(h, \chi), \quad (1)$$

with

$$f(h, \chi) = \xi_h h^2 + \xi_\chi \chi^2, \quad (2)$$

and

$$V(h, \chi) = \frac{\lambda}{4} (h^2 - \alpha \chi^2)^2 + \beta \chi^4 \quad (3)$$

a scale-invariant potential with  $\alpha \geq 0$ ,  $\beta \geq 0$ . In order to have a well-defined graviton propagator for all field values, the non-minimal couplings  $\xi_h$  and  $\xi_\chi$  must be positive definite,  $\xi_h, \xi_\chi > 0$ . The Lagrangian density (1) is supplemented with the SM Lagrangian density without the Higgs potential,  $\mathcal{L}_{\text{SM}[\lambda \rightarrow 0]}$ . Apart from a potential dark matter candidate, no additional degrees of freedom are added on top of this minimalistic matter content.

In the absence of gravity, the ground state of the Higgs-Dilaton system corresponds to the minima of the scale-invariant potential (3). For  $\alpha \neq 0$  and  $\beta = 0$ , this potential contains two flat directions with

$$h_0^2 = \alpha \chi_0^2, \quad (4)$$

and arbitrary  $\chi_0$  that lead to the spontaneous symmetry breaking of scale invariance. The case  $\beta \neq 0$  translates into a physically unacceptable ground state,  $h_0 = \chi_0 = 0$ , containing a massless Higgs boson and no electroweak symmetry breaking.

The inclusion of gravity via the non-minimal couplings  $\xi_h$  and  $\xi_\chi$  results in the appearance of an additional ground state

$$h_0^2 = \alpha \chi_0^2 + \frac{\xi_h}{\lambda} R. \quad (5)$$

Depending on the value of  $\beta$ , the background spacetime corresponds to a flat ( $\beta = 0$ ), de Sitter ( $\beta > 0$ ) or anti de Sitter ( $\beta < 0$ ) geometry,

$$R = \frac{4\beta \chi_0^2}{\xi_\chi + \alpha \xi_h}. \quad (6)$$

Among the possible values of  $\beta$ , the case  $\beta = 0$  seems to be preferred from the quantum field theory point of view. Indeed, the presence of the massless scalar field  $\chi$  in both de Sitter and anti de Sitter backgrounds is known to give rise to instabilities [32, 33], see also Refs. [34–38]. These results seem to be in conceptual agreement with those following from functional renormalization group approaches involving non-minimally coupled scalar fields [39]. On top of that, the case  $\beta = 0$  allows for the spontaneous symmetry breaking of scale invariance *even in the absence of gravity*. Based on these arguments, we will focus on the  $\beta = 0$  case in what follows.

In unimodular gravity [40–46] the metric determinant in Eq. (1) is restricted to take a constant value  $g = -1$ . As General Relativity, UG can be understood as a particular case of a theory invariant under transverse diffeomorphisms,  $x^\mu \rightarrow x^\mu + \xi^\mu$  with  $\partial_\mu \xi^\mu = 0$ , in which the third metric degree of freedom is absent [42, 47, 48]. Note

that the unimodular constraint is not a strong restriction since the resulting theory of gravity can still describe all possible geometries.

The presence of the unimodular constraint  $g = -1$  translates into the appearance of an integration constant  $\Lambda_0$  at the level of the equations of motion [5]. These equations coincide with those obtained from a *diffeomorphism invariant* Lagrangian [5]

$$\frac{\mathcal{L}}{\sqrt{-g}} = \frac{f(h, \chi)}{2} R - \frac{1}{2} (\partial h)^2 - \frac{1}{2} (\partial \chi)^2 - V(h, \chi) + \Lambda_0, \quad (7)$$

but with  $\Lambda_0$  understood as an initial condition rather than a cosmological constant. Given the equivalence of the two formulations, we will work with the more familiar diffeomorphism invariant Lagrangian (7), but keeping in mind the aforementioned interpretation of  $\Lambda_0$ .

## A. Higgs-Dilaton Cosmology

As explained in the previous section any solution with  $\beta = 0$  and  $\chi_0 \neq 0$  leads to the spontaneous symmetry breaking of scale invariance. The expectation value of the field  $\chi$  induces the masses of the SM particles through its coupling to the Higgs field and defines the effective Planck mass. The hierarchy between the Planck mass  $M_P$  and the electroweak scale  $v$  is reproduced by properly fine-tuning the  $\alpha$  coupling to a value  $\sim v^2/M_P^2 \sim 10^{-32}$  [5, 6]. Due to the small value of this coupling constant, the flat directions in Eq. (4) are essentially aligned with the direction of the  $\chi$  field. For all practical purposes it will be enough to consider the Lagrangian density (7) in the  $\alpha \simeq 0$  approximation, but keeping in mind that the potential really contains two almost-degenerate valleys.

The cosmological consequences of the HD model are more easily understood in the so-called Einstein frame, in which the gravitational part of the action takes the usual Einstein-Hilbert form. Performing a metric rescaling  $g_{\mu\nu} \rightarrow \Omega^{-2} g_{\mu\nu}$  with conformal factor

$$\Omega^2 = f(h, \chi)/M_P^2, \quad (8)$$

we obtain the Einstein-frame Lagrangian density

$$\frac{\mathcal{L}}{\sqrt{-g}} = \frac{M_P^2}{2} R - \frac{1}{2} g^{\mu\nu} \gamma_{ab} \partial_\mu \varphi^a \partial_\nu \varphi^b - U_E(\varphi^a), \quad (9)$$

where we have made use of a compact notation  $\varphi^a = (\varphi^1, \varphi^2) = (h, \chi)$  to define a field-space metric

$$\gamma_{ab} = \frac{1}{\Omega^2} \left( \delta_{ab} + \frac{3}{2} M_P^2 \frac{\partial_a \Omega^2 \partial_b \Omega^2}{\Omega^2} \right). \quad (10)$$

The Einstein-frame potential  $U_E = U + U_{\Lambda_0}$  is given by the sum of two pieces,

$$U(h, \chi) = \frac{\lambda}{4} \frac{M_P^4 h^4}{f^2(h, \chi)}, \quad U_{\Lambda_0}(h, \chi) = \frac{\Lambda_0 M_P^4}{f^2(h, \chi)}, \quad (11)$$

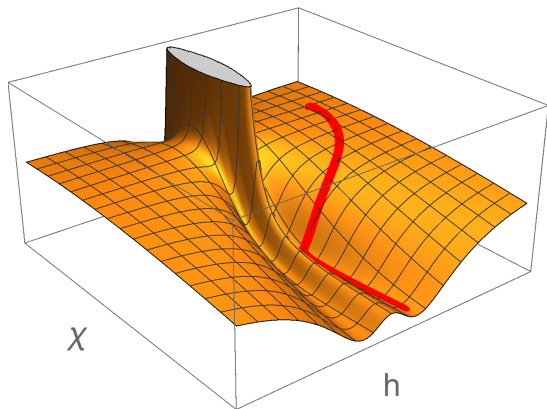


FIG. 1. The HD Einstein-frame potential  $U_E = U + U_{\Lambda_0}$  in the  $\Lambda_0 > 0$  case. In order to better visualize the almost degenerate valleys at  $h_0 = \pm\sqrt{\alpha}\chi_0$  we used a rather large and unphysical value of  $\alpha$ . For illustration purposes we also included a typical Higgs-Dilaton trajectory. Inflation takes place in the asymptotically flat region, where the effective potential can be well approximated by the  $U$  term and scale-invariance is approximately realized. The conservation of the Noether current associated to this continuous symmetry restricts the motion of the fields to ellipsoidal trajectories in the  $\{h, \chi\}$  plane. After inflation, heating and entropy production take place and the fields eventually relax to the valleys of the potential. Due to the  $U_{\Lambda_0}$  term in Eq. (11), these valleys are slightly tilted towards  $\chi \rightarrow \infty$ . At early times, the Hubble friction is so large that the fields stay essentially “frozen”. When the decreasing SM energy density equals the approximately constant term  $U_{\Lambda_0}$ , the fields roll down the valley and asymptotically approach the ground state of the system at  $\chi \rightarrow \infty$ .

whose effect is illustrated in Fig. 1. The term  $U_{\Lambda_0}$  modifies the flat directions (4) associated to the spontaneous symmetry breaking of scale invariance. For  $\Lambda_0 < 0$  the vacuum valleys become tilted towards the origin, leading to a trivial ground state with  $\chi = h = 0$  and no particle excitations. For  $\Lambda_0 > 0$ , the ground state of the system is rather located at  $\chi \rightarrow \infty$ . Far away from the symmetry-breaking valleys, the contribution  $U_{\Lambda_0}$  becomes negligible and the effective potential  $U_E$  can be well approximated by the  $U$  term, which becomes asymptotically flat for sufficiently large values of the Higgs field.

The non-diagonal metric in Eq. (9) can be recast into a diagonal form by considering an additional field redefinition  $\{h, \chi\} \rightarrow \{\Theta, \Phi\}$  with

$$\gamma^{-2}\Theta \equiv \frac{(1+6\xi_h)h^2 + (1+6\xi_\chi)\chi^2}{\xi_h h^2 + \xi_\chi \chi^2}, \quad (12)$$

$$\exp\left[\frac{2\gamma\Phi}{M_P}\right] \equiv \frac{\kappa_c(1+6\xi_h)h^2 + (1+6\xi_\chi)\chi^2}{M_P^2}. \quad (13)$$

For future convenience we have also defined several non-

minimal coupling combinations, namely

$$\kappa_c \equiv -\frac{\xi_h}{1+6\xi_h}, \quad \kappa \equiv \kappa_c \left(1 - \frac{\xi_\chi}{\xi_h}\right), \quad (14)$$

and

$$\gamma \equiv \sqrt{\frac{\xi_\chi}{1+6\xi_\chi}}. \quad (15)$$

Note that the variable  $\Theta$  in Eq. (12) is a function of the ratio of  $h$  to  $\chi$  and thus it does not transform under scale transformations. This type of transformations acts only on the  $\Phi$  field, which can be interpreted as a generalized radial coordinate in the  $\{h, \chi\}$  plane. This variable is defined in such a way that scale transformations act on it as shift transformations. In terms of the coordinates  $\{\Theta, \Phi\}$ , the Lagrangian density (9) becomes

$$\frac{\mathcal{L}}{\sqrt{-g}} = \frac{M_P^2}{2}R - \frac{K(\Theta)}{2}(\partial\Theta)^2 - \frac{\Theta}{2}(\partial\Phi)^2 - U - U_{\Lambda_0}, \quad (16)$$

with

$$U(\Theta) = U_0(1-\Theta)^2, \quad U_{\Lambda_0}(\Theta, \Phi) = \frac{\Lambda_0}{c^2}\Theta^2 e^{-\frac{4\gamma\Phi}{M_P}}, \quad (17)$$

and

$$U_0 \equiv \frac{\lambda a^2 M_P^4}{4}, \quad a \equiv \frac{1+6\kappa}{\kappa}, \quad c \equiv \frac{\kappa}{\kappa_c}\gamma^2. \quad (18)$$

For sufficiently large values of  $\Phi$ , the symmetry-breaking potential  $U_{\Lambda_0}$  becomes negligible as compared to  $U$ . In this limit, the field  $\Phi$  is only derivatively coupled and the action acquires an emergent shift symmetry  $\Phi \rightarrow \Phi + C$  with  $C$  a constant. This symmetry can be understood as the non-linear realization of the original scale invariance and allows to interpret the field  $\Phi$  as the Goldstone boson, or dilaton, associated to its spontaneous symmetry breaking. The dominant term  $U$  approaches a constant value  $U_0$  at small  $\Theta$  values and allows for inflation with the usual chaotic initial conditions.

Note that Eq. (16) contains a non-canonical coefficient for the  $\Theta$ -field kinetic term,

$$K(\Theta) = -\frac{M_P^2}{4\Theta} \left( \frac{1}{\kappa\Theta + c} + \frac{a}{1-\Theta} \right), \quad (19)$$

which could easily be removed by performing a simple field redefinition of the  $\Theta$  field,  $\bar{\Theta} \equiv \int \sqrt{K(\Theta)}d\Theta$ . The structure of  $K(\Theta)$  is, however, particularly enlightening. It contains three poles at  $\Theta = 0$ ,  $\Theta = -c/\kappa$  and  $\Theta = 1$ . While the first two poles are potentially explored during inflation, the  $\Theta = 1$  pole is just a “Minkowski” pole in which the conformal factor (8) approaches one and the usual SM non-minimally coupled to gravity is approximately recovered. For the field values relevant for inflation, the “Minkowski” pole can be safely neglected. In this limit, the field-derivative manifold in Eq. (16) becomes a maximally symmetric space with Gaussian curvature  $\kappa$  [49]. As we will see below, this highly symmetric

structure has a strong impact on the inflationary observables.

Given the above considerations a simple overall picture emerges. With the standard slow-roll initial conditions within the plateau region in Fig. 1, the inflaton field  $\Theta$  will tend to roll down the  $U(\Theta)$  potential. While this happens ( $\Theta \simeq 0$ ), the  $\Phi$ -field kinetic term is effectively suppressed and the dilaton “freezes” at its initial value  $\Phi = \Phi_0$ . This is an immediate consequence of scale-invariance. Indeed, as shown in Ref. [6], the conservation of the Noether current associated to this continuous symmetry restricts the motion of the  $h$  and  $\chi$  fields to  $\Phi = \text{constant}$  ellipsoidal trajectories in the  $\{h, \chi\}$  plane (cf. Fig. 1). This means that, in spite of dealing with a two-field model of inflation, no isocurvature perturbations nor non-Gaussianities are produced. For all practical purposes, the HD model behaves as a *single-field* inflationary model [6]. After the end of inflation, entropy production takes place along the lines of Refs. [50–52]. Once the heating stage is complete, the field  $\Theta$  settles down at the minimum of the  $U$  potential. The expectation value of  $\Theta$  at this minimum,  $\Theta_0 = \Theta[h_0/\chi_0]$ , translates into constant values for the masses of the SM particles produced during the heating stage. The radiation and matter dominated epochs proceed therefore in the standard way. During these eras, the almost massless scalar field  $\Phi$  behaves essentially as a thawing quintessence field [1, 53–55]. In particular, it stays “frozen” until the decreasing energy density in the SM sector equals the approximately constant term  $U_{\Lambda_0}$ . When that happens, the field starts rolling down this exponential potential and the Universe enters a dark energy dominated era. In the following sections we discuss each of these epochs in detail.

## B. Inflation

As argued in the previous section we can neglect the symmetry breaking potential  $U_{\Lambda_0}$  and the “Minkowski” pole at  $\Theta = 1$  for the field values relevant for inflation. Given the resulting action, the inflationary observables can be computed using the standard techniques. Parametrizing the spectrum of scalar and tensor perturbations generated during inflation in the almost scale-invariant form [56]

$$P_s = A_s \left( \frac{k}{k_*} \right)^{n_s - 1 + \frac{1}{2} \alpha_s \ln\left(\frac{k}{k_*}\right)}, \quad P_t = A_t \left( \frac{k}{k_*} \right)^{n_t}, \quad (20)$$

and using the slow-roll approximation for a non-canonical inflaton field  $\Theta$ , we get

$$A_s = \frac{1}{24\pi^2 M_P^4} \frac{U}{\epsilon}, \quad n_s = 1 + 2\eta - 6\epsilon, \quad (21)$$

$$\alpha_s = 8\epsilon(2\eta - 3\epsilon) - 2\delta^2, \quad r \equiv \frac{A_t}{A_s} = -8n_t = 16\epsilon, \quad (22)$$

with

$$\epsilon \equiv \frac{M_P^2}{2K} \left( \frac{U, \Theta}{U} \right)^2, \quad \eta \equiv \frac{M_P^2}{\sqrt{KU}} \left( \frac{U, \Theta}{\sqrt{K}} \right)_{, \Theta}, \quad (23)$$

$$\delta^2 \equiv \frac{M_P^4 V, \Theta}{KV^2} \left[ \frac{1}{\sqrt{K}} \left( \frac{V, \Theta}{\sqrt{K}} \right)_{, \Theta} \right]_{, \Theta}, \quad (24)$$

the slow-roll parameters and  $_{, \Theta}$  denoting a derivative with respect to  $\Theta$ . The inflationary observables (21) and (22) are understood to be evaluated at a field value  $\Theta_* \equiv \Theta(N_*)$ . The quantity  $N_*$  stands for the number of  $e$ -folds before the end of inflation at which the reference pivot scale  $k_*$  in Eq. (20) exited the horizon,  $k_* = a_* H_*$ . Using the first slow-roll parameter from Eq. (23) together with the standard relation for the number of  $e$ -folds  $N_*$  as a function of the non-canonical field  $\Theta_*$ ,

$$N_* = \frac{1}{M_P} \int_{\Theta_*}^{\Theta_E} \frac{\sqrt{K} d\Theta}{\sqrt{2\epsilon}}, \quad (25)$$

we obtain

$$N_* = \frac{1}{8c} \ln \left[ \frac{\Theta_*}{\Theta_E} \left( \frac{\kappa \Theta_E + c}{\kappa \Theta_* + c} \right)^{1 + \frac{c}{\kappa}} \right], \quad (26)$$

with

$$\Theta_E = \frac{1 - 4c - 2\sqrt{4c^2 - 2c - 2\kappa}}{1 + 8\kappa} \quad (27)$$

the value of the field at the end of inflation,  $\epsilon(\Theta_E) \equiv 1$ . To invert Eq. (26) we assume the ratio  $c/|\kappa|$  to be small and perform a Taylor expansion around  $c/|\kappa| \approx 0$ . In terms of the original fields  $h$  and  $\chi$ , this corresponds to an inflationary dynamics which is essentially dominated by the Higgs component, i.e. with  $\xi_h \gg \xi_\chi$  or equivalently with  $|\kappa| \simeq |\kappa_c|$ , cf. Eq. (14). To the lowest order in  $c/|\kappa|$  we obtain the following analytical expressions for the amplitude of the primordial spectrum of scalar perturbations,

$$A_s = \frac{\lambda \sinh^2(4cN_*)}{1152\pi^2 \xi_{\text{eff}}^2 c^2}, \quad \xi_{\text{eff}} \equiv \frac{1}{\sqrt{6a^2 |\kappa_c|}}, \quad (28)$$

the spectral tilt and its running

$$n_s = 1 - 8c \coth(4cN_*), \quad (29)$$

$$\alpha_s = -32c^2 \text{csch}^2(4cN_*), \quad (30)$$

and the tensor-to-scalar ratio

$$r = \frac{32c^2}{|\kappa_c|} \text{csch}^2(4cN_*). \quad (31)$$

Note that the spectral tilt is bounded from above and that the observables (29)-(31) are non-trivially related,

$$n_s \lesssim 1 - \frac{2}{N_*}, \quad r \leq \frac{(n_s - 1)^2}{2|\kappa_c|}, \quad \alpha_s = -|\kappa_c| r. \quad (32)$$

As long as the quantity  $4cN_*$  is smaller than one, the series expansions of the hyperbolic functions in Eqs. (29)-(31) rapidly converge and we can further approximate them by

$$n_s \simeq 1 - \frac{2}{N_*}, \quad \alpha_s \simeq -\frac{2}{N_*^2}, \quad r \simeq \frac{2}{|\kappa_c|N_*^2}. \quad (33)$$

The structure of these equations is a natural consequence of the pole structure in Eq. (19) [49]. In the limit  $c \rightarrow 0$ , the pole in this expression becomes approximately quadratic. This behavior translates into an exponential flattening of the  $U$  potential when written in terms of a canonically normalized field  $\bar{\Theta} \equiv \int \sqrt{K(\Theta)}d\Theta$ . The quadratic pole acts as an attractor driving the inflationary observables towards the values (33). Note that for not too small  $|\kappa_c|$ , the tensor-to-scalar ratio is highly suppressed,  $r \sim \mathcal{O}(10^{-3})$ . This shares similarities with the  $\alpha$ -attractors discussed in Refs. [21–23] (for a connection between this approach and the existence of stationary points along the inflationary potential see Ref. [57]).

For  $4cN_*$  larger than one the inflationary observables (29)-(31) approach the *asymptotic* values

$$n_s \simeq 1 - 8c, \quad \alpha_s \simeq 0, \quad r \simeq 0. \quad (34)$$

This limit is again a natural consequence of the pole structure in Eq. (19) [49]. Indeed, for  $c \neq 0$ , the inflationary pole at  $\Theta = 0$  is no longer reachable and we are left with a linear pole structure. As shown in Ref. [58], the linear pole also acts as an effective attractor driving the inflationary observables towards the values (34).

### C. Heating and entropy production

The precise value of  $N_*$  in Eqs. (28)-(31) depends on the duration of the heating stage. The heating stage in Higgs-Dilaton inflation coincides with that in Higgs inflation [50, 51], up to a negligible dilaton production<sup>1</sup> associated to the non-canonical kinetic term in Eq. (16) [6, 59]. After the end of inflation the  $\Theta$  field starts to oscillate around the minimum of  $U$ . These oscillations lead to the production of  $W^\pm$  and  $Z$  gauge bosons which tend to decay upon production into the Standard Model quarks and leptons. The decay probability is proportional to the gauge boson effective mass, which depends itself on the  $\Theta$ -field expectation value. The large amplitude of the

<sup>1</sup> The Goldstone boson nature of the dilaton makes it a potential candidate for contributing to the effective number of relativistic degrees of freedom at Big Bang Nucleosynthesis and recombination. However, the extremely small production of this component during the reheating stage translates into a number of degrees of freedom very close to the Standard Model one [59]. For all practical purposes, the dilaton *excitations* remain elusive and completely undetectable by any particle physics experiment or cosmological observation. The only remnant of the dilaton *field* is a dynamical dark energy stage, cf. Section II D.

dynamical field  $\Theta$  at the onset of the heating stage translates into a very efficient decay which tends to deplete the gauge boson occupation numbers within a single oscillation and delays the onset of parametric resonance [50, 51]. As the Universe expands, the average value of  $\Theta$  decreases and eventually becomes small enough as to allow for the gauge bosons to accumulate. When that happens, the system enters into a parametric resonance regime and eventually backreacts into the inflaton condensate. From there on until thermalization, the evolution of the system is very non-linear and non-perturbative and one must rely on lattice simulations [60]. The different analytical and numerical considerations in Refs. [6, 50, 51, 60] seem to indicate that heating in Higgs-Dilaton inflation takes place rather fast, leading to a relatively well-constrained number of  $e$ -folds,<sup>2</sup>  $60 \lesssim N_* \lesssim 62$ .

### D. Dark energy

Given the value of the Higgs self-coupling at the inflationary scale<sup>3</sup> and the aforementioned duration of the heating stage, the values of  $|\kappa| \simeq |\kappa_c|$  and  $c$  (or equivalently of the non-minimal couplings  $\xi_h$  and  $\xi_\chi$ ) can be fixed by comparing the inflationary predictions (28)-(31) with cosmic microwave background (CMB) data. The free parameters of the model then become completely determined. This allows us to make specific predictions for any subsequent period in the evolution of the Universe. In particular, it is possible to derive an extremely appealing connection between inflation and the present dark energy dominated era. Establishing this connection is the purpose of this section.

After the end of the reheating stage, the field  $\Theta$  will relax towards the minimum of  $U$ . When this happens, the Higgs-Dilaton action (16) boils down to the simple Lagrangian density

$$\frac{\mathcal{L}}{\sqrt{-g}} \simeq \frac{M_P^2}{2}R - \frac{1}{2}(\partial\Phi)^2 - \frac{\Lambda_0}{c^2}e^{-\frac{4\gamma\Phi}{M_P}}, \quad (35)$$

supplemented by the Lagrangian density for the matter and radiation components produced during the heating stage [50, 51, 60].

If  $\Lambda_0 > 0$ , the potential for the dilaton field is of the runaway-type and can support an accelerated expansion of the Universe while driving  $\Phi \rightarrow \infty$ . This type of potential was first considered in the seminal papers [1, 2]. Regarding the late time acceleration of the Universe, the *cosmon scenario* presented there displays some formal similarities with the HD model but at the same time

<sup>2</sup> We use the Planck satellite pivot scale  $k_* = 0.05/\text{Mpc}$  rather than  $k_* = 0.002/\text{Mpc}$ . This translates into a shift of roughly three  $e$ -folds with respect to the estimates in Ref. [6].

<sup>3</sup> For details cf. Ref. [61]. For the HD model the behavior near the critical point has been studied in Ref. [62].

some conceptual differences. In Refs. [1, 2] the runaway potential in Eq. (35) appears as a consequence of the dilatation anomaly and therefore of the explicit breaking of scale invariance. In the HD model, scale-invariance is assumed to be an exact symmetry at the quantum level and the exponential potential appears as a consequence of the unimodular character of gravity.

The quintessence potential in the Higgs-Dilaton scenario is nearly flat and the quintessence fluid started to dominate only recently. We are thus dealing with a thawing quintessence scenario [54, 55]. The evolution equations for the dilaton/matter system can be written as [63–65]

$$\frac{w'}{1-w} = -3(1+w) + 4\gamma\sqrt{3(1+w)\Omega_{\text{DE}}}, \quad (36)$$

$$\Omega'_{\text{DE}} = -3\Omega_{\text{DE}}(1 - \Omega_{\text{DE}})w, \quad (37)$$

with  $\Omega_{\text{DE}}$  the dark-energy energy density parameter associated to the dilaton field  $\Phi$ ,  $w$  its effective equation-of-state parameter and the primes denoting derivatives with respect to the number of  $e$ -folds  $N = \ln a$ . During matter and radiation domination the density parameter  $\Omega_{\text{DE}}$  is small and the last term in Eq. (36) can be safely neglected. The dilatonic dark energy component then behaves as a (subdominant) cosmological constant with an equation-of-state parameter  $w \simeq -1$ . However, since the dilaton energy density remains approximately constant, the fraction  $\Omega_{\text{DE}}$  will eventually become relevant. As shown in Refs. [1, 54, 66], the set of equations (36) and (37) admits a stable fixed point,

$$\Omega_{\text{DE}} = 1, \quad 1+w = \frac{16\gamma^2}{3}, \quad (38)$$

which leads to acceleration if  $\gamma < 1/(2\sqrt{2})$ . Indeed, in the approximation  $1+w \ll 1$ , we can easily integrate Eqs. (36) and (37) to obtain [64]

$$1+w = \frac{16\gamma^2}{3}F(\Omega_{\text{DE}}), \quad \Omega_{\text{DE}} = \frac{1}{1 + \Delta_0 a^{-3}}, \quad (39)$$

with

$$F(\Omega_{\text{DE}}) = \left[ \frac{1}{\sqrt{\Omega_{\text{DE}}}} - \Delta \tanh^{-1} \sqrt{\Omega_{\text{DE}}} \right]^2, \quad (40)$$

and

$$\Delta \equiv \frac{1 - \Omega_{\text{DE}}}{\Omega_{\text{DE}}}, \quad \Delta_0 \equiv \frac{1 - \Omega_{\text{DE},0}}{\Omega_{\text{DE},0}}. \quad (41)$$

The subscript 0 marks quantities evaluated today. The function  $F(\Omega_{\text{DE}})$  is a monotonically increasing function smoothly interpolating between  $F(0) = 0$  in the deep radiation and matter dominated eras and  $F(1) = 1$  in the asymptotic dark energy dominated era. The present value of the dark-energy equation-of-state parameter follows directly from Eq. (39),

$$\frac{1+w_0}{1+w(a)} = \frac{F(\Omega_{\text{DE},0})}{F(\Omega_{\text{DE}})}. \quad (42)$$

## E. Consistency relations

Note that the equation-of-state parameter in Eq. (39) depends only on  $\gamma$ , which coincides with  $\sqrt{c}$  in the  $|\kappa| \approx |\kappa_c|$  approximation. Combining this expression with Eq. (29) we get the following consistency relation between the spectral tilt of scalar perturbations generated during inflation and the equation-of-state parameter of dark energy, namely

$$n_s = 1 - \frac{2}{N_*} X \coth X, \quad (43)$$

with

$$X \equiv 4cN_* = \frac{3N_*(1+w)}{4F(\Omega_{\text{DE}})}. \quad (44)$$

A similar consistency relation can be derived for the running of the spectral tilt,  $\alpha_s = -|\kappa_c|r$ , and the tensor-to-scalar ratio

$$r = \frac{2}{|\kappa_c|N_*^2} X^2 \sinh^{-2} X. \quad (45)$$

The validity of the consistency relations (43) and (45) is restricted to the range of validity of the approximation  $c/|\kappa| \ll 1$ . The derivation presented in this paper allows for a straightforward generalization to general scale-invariant scenarios as those considered in Ref. [49]. For the particular model under consideration, the constant  $|\kappa| \simeq |\kappa_c|$  is determined by the amplitude of the primordial power spectrum (28) once the value of the Higgs self-coupling at the inflationary scale is specified. For the values of  $\lambda$  following from the usual SM renormalization group running [67–70], one gets  $\xi_{\text{eff}} \simeq \xi_h \gg 1$ , which leads to a value  $|\kappa| \simeq |\kappa_c| \simeq 1/6$  for the field-derivative space curvature. In this limit, the expressions (43) and (45) reduce to those in Ref. [6].

Whether the consistency relations (43) and (45) remain unaltered or rather become modified in the presence of quantum corrections depends on the particular UV completion of the Standard Model non-minimally coupled to gravity. A potential UV completion respecting the symmetries of the non-renormalizable action (1) was conjectured in Refs. [5, 17]. The bottom-up approach of Refs. [71, 72] shows that it is indeed possible to remove all the divergencies in the theory while keeping scale invariance intact. The price to pay is the lack of renormalizability [73], which does not seem to be a strong requirement given that gravity itself is non-renormalizable. For scale-invariant UV completions, the consistency relations (43) and (45) remain unaltered [8]. Deviations from these consistency relations are only expected in the so-called critical regime in which the Higgs-Dilaton potential develops an inflection point along the inflationary trajectory [62] (see also Refs. [74–76]).

Parameter	Description	Prior range	$\Lambda$ CDM	HD	$w$ CDM
$\omega_b = \Omega_b h^2$	Baryon density today	[0.005, 0.1]	•	•	•
$\omega_{cdm} = \Omega_{cdm} h^2$	CDM density today	[0.001, 0.99]	•	•	•
$h$	Dimensionless Hubble constant	[0.1, 2]	•	•	•
$\ln(10^{10} A_s)$	Amplitude of primordial curvature perturbations	[2, 4]	•	•	•
$\tau_{reio}$	Optical depth due to reionization	[0.01, 0.8]	•	•	•
$n_s$	Spectral tilt	[0.8, 1.2]	•		•
$r$	Tensor-to-scalar ratio	[0.0, 0.5]	•		•
$w_0$	Current value of the dark energy equation of state	[-1, 0]		•	•
$N_*$	Number of $e$ -folds of inflation w.r.t. $k = 0.05 \text{ Mpc}^{-1}$	$(60 \pm 2.5)$		•	
$\Sigma m_\nu$	Sum of neutrino masses	[0.0, 5.0]	•	•	•

TABLE I. The priors used in the MCMC analysis. The dots indicate the parameters that are varied as independent parameters in the given model. For the number of  $e$ -folds  $N_*$ , we implement a strong Gaussian prior (see the text). We choose flat priors for the other parameters.

### III. CURRENT DATA

The Higgs-Dilaton consistency relations derived in the previous section bring us to an unusual situation in which some cosmological observables that are customarily understood as independent parameters become related in a rather non-trivial manner. In a Higgs-Dilaton cosmology, a dynamical dark energy component is inevitably associated to deviations from the  $\alpha$ -attractor predictions in Eq. (33). To understand the impact of the consistency relations on cosmological observables we will consider three different scenarios:

1. A standard  $\Lambda$ CDM cosmology.
2. A HD model satisfying the consistency relations (43)-(45) between the dark-energy equation-of-state parameter, the spectral tilt and the tensor-to-scalar ratio.
3. A  $w$ CDM model satisfying the thawing quintessence condition (42) but without any additional constraints on the primordial power spectra.

By comparing the HD model to  $\Lambda$ CDM, we will explore how the observables in the former scenario differ from those in the standard cosmological picture. The comparison of the HD model with a  $w$ CDM cosmology will allow us to isolate the impact of the consistency relations.

#### A. Parameters and priors

For each of the aforementioned models we follow the conventional Bayesian approach for the estimation of cosmological parameters and perform a Markov Chain Monte Carlo (MCMC) analysis. The iterative MCMC algorithm samples the parameter space weighted by a prior distribution by constructing a Markov chain whose

equilibrium distribution is the target posterior distribution. The quality of the sampling improves with the number of steps. After sampling for a sufficiently long time, the chain reaches equilibrium and the samples can be regarded as those from the desired posterior distribution. The varying parameters in the  $\Lambda$ CDM, HD and  $w$ CDM scenarios are summarized in Table I. For all cases, we assume an exactly flat Universe with  $\Omega_K = 0$ , three degenerate massive neutrinos and no additional sterile neutrino species. In the HD case we vary only the present dark-energy equation-of-state parameter and use the consistency relations (43)-(45) to compute the spectral tilt and the tensor-to-scalar ratio from it. Doing so implies adding the number of  $e$ -folds of inflation as a free parameter. For the  $w$ CDM case we adopt the dark-energy evolution (42) but without implementing any additional constraint or consistency relation on the primordial power spectra. Since the spectral tilt and the tensor-to-scalar ratio are free parameters in this case, the number of  $e$ -folds does no longer play any role.

As argued in Section II C, all HD model estimates predict a rapid entropy production after inflation leading to a number of  $e$ -folds  $N_* \simeq 60$ , with an uncertainty of a few  $e$ -folds. To account for the theoretical knowledge of this heating stage we implement a strong theoretical prior for the number of  $e$ -folds of inflation. In particular, we choose a Gaussian prior with central value  $\mu = 60$  and standard deviation  $\sigma = 2.5$ . For the rest of the parameters we implement flat priors with boundaries as given in Table I. Since the HD model does not allow for a phantom behavior  $w < -1$ , we restrict the current dark-energy equation-of-state to be larger than  $-1$ . We also apply this restriction to the  $w$ CDM case to compare the two models on equal footing.

## B. MCMC analysis

To perform the MCMC analysis we make use of the MontePython code [77]. This code is a MCMC cosmological parameter extraction code containing the most recent observational likelihoods and interfaced with the Cosmic Linear Anisotropy Solver Software (CLASS) for the computation of cosmological observables [78]. To implement the constraints described in Section II E we have modified the CLASS code in two ways. First, we have implemented the thawing quintessence evolution (42) for the equation-of-state parameter  $w(a; w_0, \Omega_{\text{DE},0})$ . This evolution is used both in the HD scenario and in the  $w$ CDM case. Second, we have modified the initial perturbations in the HD case to choose the spectral tilt and the tensor-to-scalar ratio as a function of the equation-of-state parameter  $w_0$  and the number of  $e$ -folds  $N_*$ , in accordance with the consistency relations (43)-(45).

We consider the following data sets: i) the 2015 Planck high-multipole TT likelihood, the Planck low-multipole polarization and temperature likelihood as well as the Planck lensing likelihood [79], ii) the Keck/Bicep2 likelihood data release 2015 [80], iii) the Joint Lightcurve Analysis [81] and iv) baryonic acoustic oscillations data sets from 6dF, BOSS and SDSS [82–84]. From these likelihoods we get 26 additional nuisance parameters.

Our MCMC analysis is similar in spirit to the one performed in Ref. [85]. However we differ from this work in multiple ways. First, we present an additional comparison of the HD model to  $\Lambda$ CDM. Second, by using the parametrization (42) for  $w(a)$  we capture the *full* thawing quintessence behavior of the Higgs-Dilaton model and avoid introducing an additional parameter  $w_a$  to account for the temporal dependence of the dark energy equation-of-state. Third, by constraining the number of  $e$ -folds, we only allow for values of this quantity that are in agreement with theoretical expectations. Finally, we do *not* allow for a phantom behavior with  $w < -1$ . A violation of the null energy condition in the HD model would imply a negative value for the non-minimal coupling  $\xi_\chi$  [cf. Eq. (39)] and therefore a negative Planck mass square,  $M_P^2 \simeq \xi_\chi \chi_0^2$  once the Higgs field settles down at the electroweak vacuum  $h_0^2 \simeq \alpha \chi_0^2$ , which is obviously unacceptable.

## C. MCMC results

In total we ran eight chains per model to obtain approximately  $\sim 2 \times 10^5$  samples per model. The results are depicted in Fig. 2 and 3, where we present histograms and correlation contours for the relevant cosmological parameters in the  $\Lambda$ CDM (red, dashed), HD (blue, solid) and  $w$ CDM (green, dotted) scenarios. To facilitate the comparison between the different models we converted the free parameter  $w_0$  in the HD case to the derived parameters  $n_s$  and  $r$  by means of the consistency relations (43)-(45).

Qualitatively one finds that the HD model resembles a  $\Lambda$ CDM cosmology with additional constraints on the spectral tilt and the tensor-to-scalar ratio, cf. Eq. (32). At current precision, the present dark energy equation-of-state parameter in the HD model is still compatible with a cosmological constant ( $w_0 = -1$ ). Note, however, that our best fit value  $w_0 = -0.997 \pm 0.003$  differs from that in Ref. [85] due to the physical requirement of having a well-defined graviton propagator at all field values. In particular, our dark-energy equation-of-state parameter is *not* phantom. The comparison of the HD model with a  $w$ CDM cosmology reveals also that the baryon fraction  $\Omega_b$  and the Hubble constant  $H_0$  are better constrained in the presence of the consistency relations (43)-(45), with ranges comparable to those in the standard  $\Lambda$ CDM case.

Given the contours for the amplitude of the curvature power spectrum  $A_s$  and the spectral tilt  $n_s$  we can immediately derive constraints for the model parameters  $\xi_{\text{eff}}$  and  $c$  using Eqs. (28) and (29). The result is shown in Fig. 4. The allowed values for the amplitude give rise to a band shape in the  $\{\xi_{\text{eff}}/\sqrt{\lambda}, c\}$  plane, whose upper limit is determined by the minimal values of the spectral tilt compatible with its  $1\sigma$  and  $2\sigma$  contours. As anticipated in section II E, a value of the Higgs-self coupling  $\lambda$  compatible with the usual SM renormalization group running,  $\lambda \sim \mathcal{O}(10^{-3})$ , translates into a sizable value of the effective coupling  $\xi_{\text{eff}}$ . In that limit,  $\xi_{\text{eff}} \simeq \xi_h \gg 1$  and  $|\kappa_c| \simeq 1/6$ .

To perform a more quantitative comparison among the different models we compute the Bayes factor for each scenario. Assuming that all models are *a priori* equally probable,  $\pi(M_{\Lambda\text{CDM}})/\pi(M) = 1$ , the Bayes factor

$$B(M) = \frac{p(\mathbf{x}|M)}{p(\mathbf{x}|M_{\Lambda\text{CDM}})} = \frac{\pi(M_{\Lambda\text{CDM}})}{\pi(M)} \frac{p(M|\mathbf{x})}{p(M_{\Lambda\text{CDM}}|\mathbf{x})} \quad (46)$$

measures the probability  $p(M|\mathbf{x})$  of a model  $M$  given current data  $\mathbf{x}$  as compared to the probability  $p(M_{\Lambda\text{CDM}}|\mathbf{x})$  of a  $\Lambda$ CDM scenario given the same data set. In interpreting this quantity we adopt the Kass and Raftery scale [86], a revision of Jeffreys scale. In this scale a value of  $|\Delta \ln B| > 3$  is understood as strong statistical evidence, translating into a relative probability of approximately 1/20 between the two models under consideration. To estimate the evidence  $p(M|\mathbf{x})$  directly from our MCMC chains we use the nearest neighbor approximation<sup>4</sup> introduced in Refs. [87, 88] and marginalize over the nuisance parameters. The Bayes factors obtained by this procedure are shown in Table II. We checked that our results are consistent with the Akaike and Bayesian information criteria.

The comparison of a HD cosmology and  $w$ CDM reveals a strong evidence for the former. There also is pos-

<sup>4</sup> The method assumes that individual points in the chain are independent. For a chain from a MCMC run this is clearly not the case. We checked that our qualitative results do not depend on the amount of thinning applied to the chains.

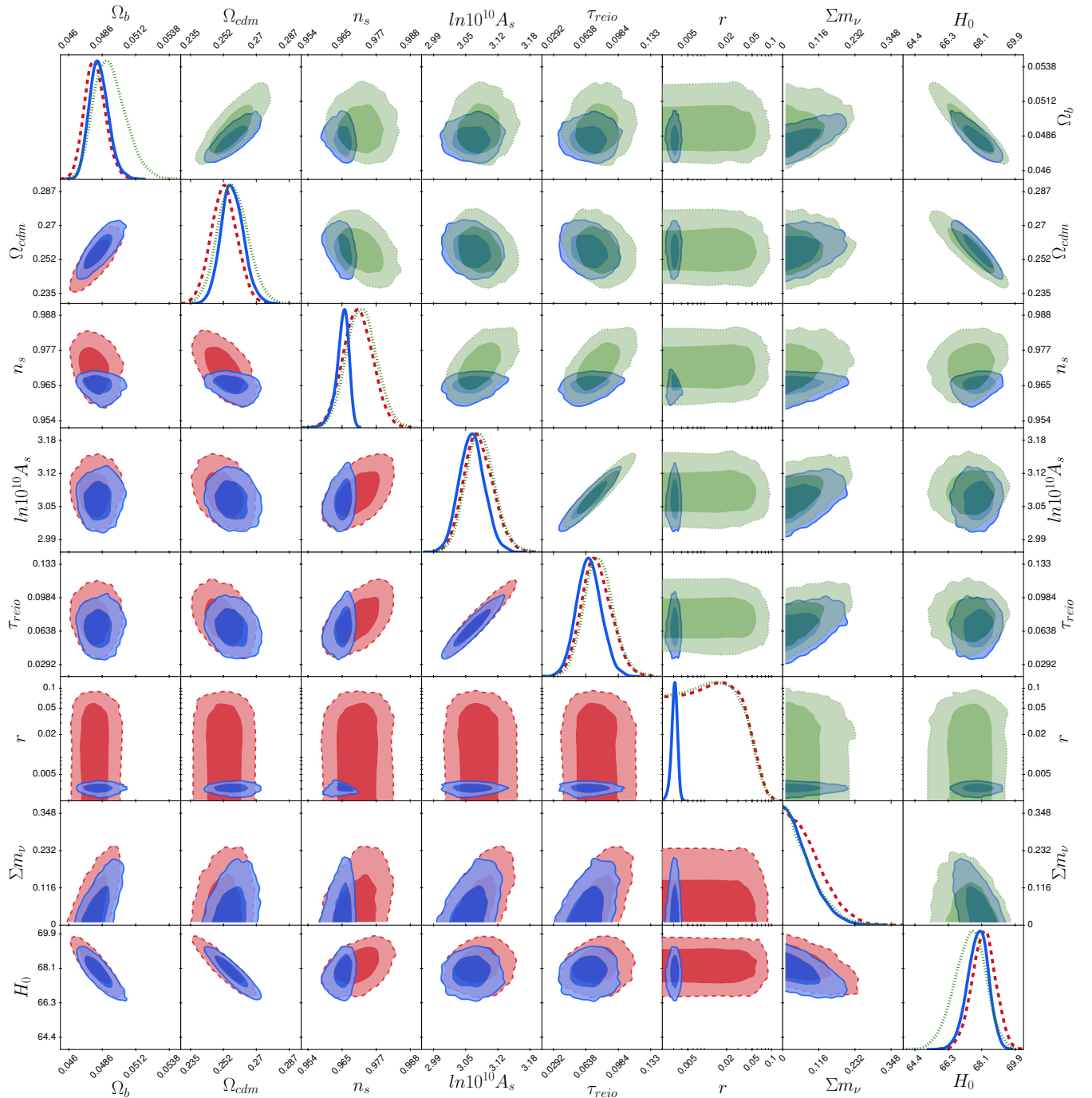


FIG. 2. Results of the MCMC run for different scenarios. The plots in the bottom left corner compare  $\Lambda$ CDM (red, dashed) with the HD model (blue, solid). The comparison of the latest scenario with  $w$ CDM (green, dotted) is shown in the upper right corner. Note that the tensor-to-scalar ratio  $r$  is plotted on a logarithmic scale (see Fig. 2 for a detailed view of the  $r$ - $n_s$  contours in the HD model).

itive evidence for  $\Lambda$ CDM over  $w$ CDM. The comparison between the HD scenario and  $\Lambda$ CDM, however, is inconclusive in the light of present data. The small difference between these two models should not be interpreted as a statistical preference for a HD cosmology since the evidence, and thus the Bayes factor, depends on the prior

volume [87, 88], which we computed for each of the models using the boundaries in Table I. If we had e.g. chosen a wider  $w_0$  prior, the preference for the HD model over  $\Lambda$ CDM would have decreased by  $\ln(\Delta w_{\text{new}}/\Delta w_{\text{old}})$ . Given the current data sets, we cannot establish a clear preference for a  $\Lambda$ CDM or a HD cosmology. This imme-

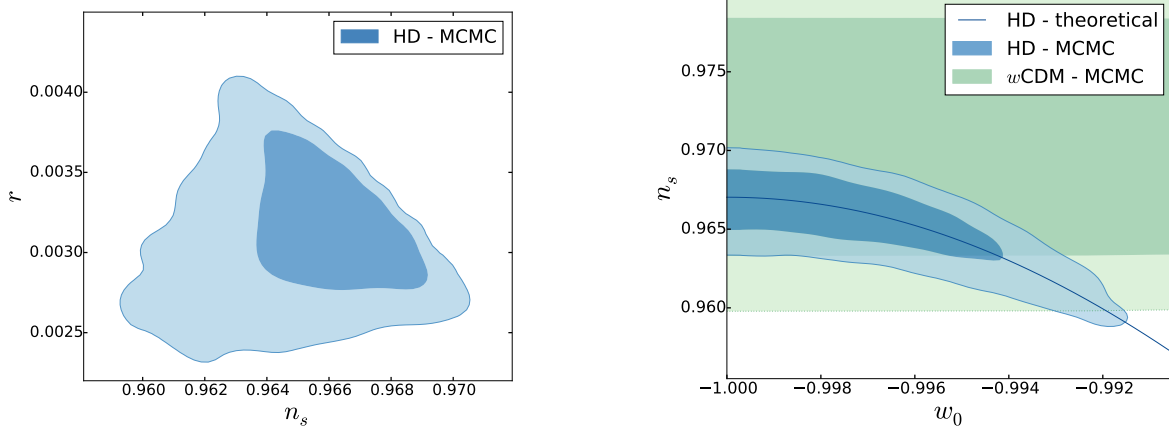


FIG. 3. (Left) Detailed view of the  $1\sigma$  and  $2\sigma$  contours for the spectral tilt and tensor-to-scalar ratio in a HD cosmology. These values are obtained by means of the consistency relations (43)-(45). This  $r$ - $n_s$  consistency relation strongly restricts the possible values for the spectral tilt  $n_s$  and the tensor-to-scalar ratio  $r$  as compared to the  $\Lambda$ CDM and  $w$ CDM scenarios (cf. Fig. 2). (Right) Detailed view of  $1\sigma$  and  $2\sigma$  contours for the spectral tilt and the present dark-energy equation-of-state in the HD model (blue, solid) and the  $w$ CDM scenario (green, dotted). The blue solid line stands for the expected HD consistency relation (43) evaluated at the mean values of the MCMC run ( $N_* = 60.7$ ,  $\Omega_{\text{DE},0} = 0.696$ ).

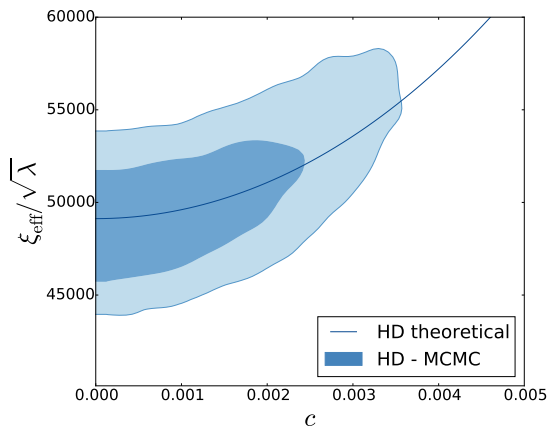


FIG. 4.  $1\sigma$  and  $2\sigma$  constraints on the model parameters  $\xi_{\text{eff}}$  and  $c$ . The contours are obtained by combining Eqs. (28) and (29) with the observationally allowed regions for the curvature power spectrum and the spectral tilt, cf. Fig. 2. The blue solid line stands for the expected HD relation evaluated at the mean values of the MCMC run ( $N_* = 60.7$ ,  $\ln(10^{10} A_s) = 3.07$ ). Note that for not too small values of the Higgs self-coupling, e.g.  $\lambda \sim \mathcal{O}(10^{-3})$ , the condition  $\xi_{\text{eff}}/\sqrt{\lambda} \gg 1$  translates into a large value of the Higgs non-minimal coupling,  $\xi_{\text{eff}} \simeq \xi_h \gg 1$ .

Model	$\Lambda$ CDM	HD	$w$ CDM
$\ln B$	0.00	0.88	-2.63

TABLE II. Maximum Likelihood estimate of the logarithm of the Bayes factor  $\ln B(M)$  with respect to  $\Lambda$ CDM. The comparison between  $\Lambda$ CDM and the HD model is inconclusive, whereas  $w$ CDM is disfavored with regard to a HD cosmology.

diately raises the question whether future surveys will be able to distinguish the two scenarios.

#### IV. FUTURE CONSTRAINTS

In this section we forecast how well the HD model can be distinguished from  $\Lambda$ CDM and  $w$ CDM using future galaxy redshift surveys. We choose three reference surveys which are planned to operate within the next decades.

As a first reference survey we will consider a DESI-like observer. DESI<sup>5</sup> is a ground-based experiment scheduled to start in 2018. It will study the large-scale structure formation in the Universe using 30 million spectroscopic redshifts and positions from galaxies and quasars [24, 25, 89]. For the forecast presented in this paper we use the specifications for the Emission Line Galaxies, as explained in Ref. [24]. The geometry and redshift binning specifications, as well as the galaxy number density and bias, can be found in Refs. [24, 90].

Our second reference survey will be a Euclid-like galaxy redshift survey [26, 27]. Euclid<sup>6</sup> is a European Space Agency mission scheduled for launch in 2020. It will measure about 2 billion photometric galaxy images and 100 million spectroscopic redshifts, providing a detailed description of structure formation up to redshift  $z \sim 2$ . To perform our forecasts we use the survey parameters for a Euclid-like mission, adapted from the Euclid Redbook specifications [27] and from Ref. [91].

<sup>5</sup> <http://desi.lbl.gov/>

<sup>6</sup> <http://www.euclid-ec.org/>

The third reference survey will be a SKA2-like galaxy survey. The Square Kilometer Array (SKA)<sup>7</sup> is an array of radiotelescopes around the globe to be built in two phases SKA1 and SKA2. Here we will use the most futuristic SKA2 stage, which is scheduled to start operating in 2030 [28–31]. The specifications for our forecast, such as geometry, bias and number density, are taken from Refs. [29, 92].

### A. Fisher analysis

To forecast the outcome of the aforementioned galaxy surveys, we use the Fisher matrix formalism [93–95], which is a fast way of approximating the curvature of the likelihood assuming that it is Gaussian on the parameters around a fiducial point. We apply this formalism to two different probes, namely Galaxy Clustering (GC) and Weak Lensing (WL), which are the main cosmological observables for next-generation galaxy surveys. We assume formulations of the likelihood which are valid in the linear regime and adapt them to partially account for the mildly non-linear effects appearing in cosmological structure formation. We also neglect cross-correlations among GC and WL, which is a conservative and rather pessimistic approach. This corresponds approximately to the Fisher matrix forecasting recipe specified in the Euclid Redbook [27].

#### 1. Galaxy Clustering

The main observable for Galaxy Clustering is the galaxy power spectrum  $P_{\text{obs}}$ , which is the Fourier transform of the two-point correlation function of galaxy number counts in redshift space. The galaxy power spectrum follows the power spectrum of the underlying dark matter distribution  $P(k)$  up to a bias factor  $b(z)$ . In this work we assume this bias factor to be local and scale-independent. Note that  $P_{\text{obs}}$  depends not only on the dark matter distribution but also on additional effects coming from the mapping between redshift space and real space, such as redshift space distortions or the pairwise peculiar velocity dispersion of galaxies, the so-called Finger-of-God effect (FoG). Neglecting further relativistic and non-linear corrections, we follow Ref. [94] and write the observed power spectrum as

$$P_{\text{obs}}(k, \mu, z) = \frac{D_{A,f}^2(z)H(z)}{D_A^2(z)H_f(z)} B^2(z) e^{-k^2 \mu^2 \sigma_{\text{tot}}^2} P(k, z), \quad (47)$$

with

$$\sigma_{\text{tot}}^2 = \sigma_r^2 + \sigma_v^2, \quad B(z) = b(z)(1 + \beta_d(z)\mu^2). \quad (48)$$

Here  $\mu \equiv \cos \varphi$ , with  $\varphi$  the angle between the line of sight and the 3D-wavevector  $\vec{k}$ . The subscript  $f$  denotes the fiducial value of each quantity,  $D_A(z)$  is the angular diameter distance,  $H(z)$  the Hubble function and  $\beta_d(z) \equiv f(z)/b(z)$ , with  $f \equiv d \ln G / d \ln a$  the linear growth rate of matter perturbations. In the exponential factor, we have a damping term  $\sigma_r^2 + \sigma_v^2$ , with  $\sigma_r$  the error induced by spectroscopic redshift measurements and  $\sigma_v$  the one associated to the FoG effect. We marginalize over this last parameter [96] and take a fiducial value  $\sigma_v = 300$  km/s compatible with the estimates in Ref. [97]. For more details on the meaning and importance of the terms in Eq. (47), the reader is referred to Refs. [90, 94, 98].

Assuming a Gaussian data covariance matrix, we can write the Fisher matrix for the galaxy power spectrum as [94, 98]

$$F_{ij} = \frac{V_{\text{survey}}}{8\pi^2} \int_{-1}^{+1} d\mu \int_{k_{\text{min}}}^{k_{\text{max}}} dk \left( \frac{\partial D}{\partial \theta_i} D^{-1} \frac{\partial D}{\partial \theta_j} D^{-1} \right), \quad (49)$$

with

$$D = D(k, \mu, z) = P_{\text{obs}}(k, \mu, z) + n(z)^{-1}. \quad (50)$$

Here  $V_{\text{survey}}$  is the volume covered by the survey and contained in a redshift slice  $\Delta z$  and  $n(z)$  is the galaxy number density as a function of redshift. The largest scales we take into account correspond to the minimum wavenumber  $k_{\text{min}} = 0.0079 \text{h/Mpc}$ . The upper limit  $k_{\text{max}}$  depends on the specifications of the survey and on the modeling of non-linear scales.

#### 2. Weak Lensing

Another important observable in future galaxy redshift surveys is the cosmic shear, which measures distortions in the ellipticities of galaxy images due to the light propagation in the Universe. For a comprehensive review, see Ref. [99]. Under the assumption of small gravitational potentials and large separations, the cosmic shear measurements can be linked to the matter power spectrum, giving access to the cosmological parameters. The cosmic shear at a redshift bin  $i$  is correlated with the cosmic shear at another redshift bin  $j$ . The power spectrum of the cosmic shear can therefore be written as a matrix with indices  $i, j$ , namely

$$C_{ij}(\ell) = \frac{9}{4} \int_0^\infty dz \frac{W_i(z)W_j(z)H^3(z)\Omega_m^2(z)}{(1+z)^4} P_m, \quad (51)$$

with  $P_m$  evaluated at the scale  $\ell/r(z)$  and  $r(z)$  the comoving distance. In this expression  $W(z)$  is a window function given by the photometric redshift distribution function and the galaxy number density distribution  $n(z)$ . For additional details on the WL formulas see, for instance, Ref. [90]. Finally, we can write the WL Fisher Matrix as a sum over all multipoles correlating the signal

<sup>7</sup> <https://www.skatelescope.org/>

Parameter	$\Lambda$ CDM	HD
$\Omega_b h^2$	$0.0223 \pm 0.0002$	$0.0223 \pm 0.0002$
$\Omega_{cdm} h^2$	$0.118 \pm 0.001$	$0.118 \pm 0.001$
$h$	$0.682 \pm 0.007$	$0.679 \pm 0.006$
$\ln(10^{10} A_s)$	$3.08 \pm 0.03$	$3.07 \pm 0.03$
$n_s$	$0.971 \pm 0.005$	$(0.966 \pm 0.003)$
$w_0$	$(-1)$	$-0.997 \pm 0.003$
$\Sigma m_\nu$	$0.08 \pm 0.08$	$0.06 \pm 0.06$

TABLE III. Fiducial values used in the Fisher analysis together with their  $1\sigma$  errors, as obtained from the MCMC analysis in Section III. The values in brackets are obtained by means of the consistency relations (43)-(45) in the HD model or by a theoretical constraint in the  $\Lambda$ CDM case. The value for  $n_s$  is only relevant for the  $\Lambda$ CDM scenario as in the HD case this value follows automatically from the  $w_0$  one.

at all redshift bins [93]

$$F_{\alpha\beta} = f_{\text{sky}} \sum_{\ell}^{\ell_{\text{max}}} \frac{(2\ell+1)\Delta\ell}{2} \text{tr} \left( \frac{\partial C}{\partial \theta_{\alpha}} \text{Cov}^{-1} \frac{\partial C}{\partial \theta_{\beta}} \text{Cov}^{-1} \right). \quad (52)$$

The prefactor  $f_{\text{sky}}$  is the fraction of the sky covered by the survey. The high-multipole cutoff  $\ell_{\text{max}}$  encodes our ignorance of clustering, systematics and baryon physics on small scales. In this work we choose  $\ell_{\text{max}} = 5000$ . The quantity

$$\text{Cov}_{ij}(\ell) = C_{ij}(\ell) + \delta_{ij} \gamma_{\text{int}}^2 \tilde{N}(n_{\theta}, \mathcal{N}_{bin})_i^{-1}(\ell) \quad (53)$$

denotes the covariance matrix of the shear power spectrum, with  $\gamma_{\text{int}}$  the intrinsic galaxy ellipticity and  $\tilde{N}_i^{-1}$  a shot noise term for each redshift bin  $i$ . This shot noise term depends on the total number of galaxies per arcmin<sup>2</sup>,  $n_{\theta}$ , and on the total number of redshift bins,  $\mathcal{N}_{bin}$  (for details see Ref. [90]).

## B. Fiducial values and numerical forecast parameters

To explore the effect of future data sets on the cosmological parameters space we first compare the HD model to a  $\Lambda$ CDM cosmology. For *each* of these two models we take the corresponding MCMC central values as fiducial values for the forecast. Second, we compare the HD scenario to a  $w$ CDM cosmology mimicking the dark-energy evolution in the Higgs-Dilaton model but without any additional constraint on the initial power spectra. In order to emphasize the impact of the consistency relations on the errors, we take the central values of the *Higgs-Dilaton* MCMC *run* as the fiducial values for *both* the HD and  $w$ CDM forecasts. For completeness, we list these values in Table III.

In each of the two aforementioned comparisons, we perform a Fisher Matrix forecast for both GC and WL

observables. To compute the derivatives needed to obtain the Fisher matrices, we use the modified version of CLASS discussed in Section IIIB and vary the relevant cosmological parameters by  $\pm 1\%$ . While the HD cosmology puts strong constraints on the running of the spectral tilt and the tensor-to-scalar ratio we do not vary them here, as they will not be directly measured by the surveys under consideration. The same applies to the optical depth  $\tau_{reio}$ , which we fix to its mean MCMC value.

In the next section we will show DESI-like, Euclid-like and SKA2-like forecasts, with different combinations of observational probes. In this work we define a DESI-like probe as a simplified GC probe accounting only for linear scales up to  $k_{\text{max}} = 0.15 \text{h/Mpc}$  but no additional non-linear corrections at baryon acoustic oscillation scales. A Euclid-like probe should be understood as the same GC probe mentioned above, but combined with a WL probe up to a maximum multipole of  $\ell_{\text{max}} = 5000$ , using a non-linear matter power spectrum and neglecting intrinsic alignment corrections. For the SKA2-like forecast, we will assume a better knowledge of the non-linear effects and use a non-linear matter power spectrum up to  $k_{\text{max}} = 0.5 \text{h/Mpc}$  for GC, while for WL we will use the same maximum multipole as in the Euclid-like case. The real constraining power of future galaxy surveys will most probably be somewhere in between the last two cases, once a better modeling of non-linear scales is taken into account and more probe combinations are added into the analysis. For GC we use the latest Halofit [100, 101] version available in the CLASS code [78] for the non-linear corrections to the matter power spectrum. This is justified since both the HD and the  $w$ CDM scenario have the same first-order matter perturbations as  $\Lambda$ CDM. We combine all forecasts with the results from the MCMC run in Section IIIC by adding the associated Fisher matrices. In doing this we neglect cross-correlations between CMB lensing and weak gravitational lensing, as well as cross-correlations between galaxy lensing and galaxy clustering, as was studied for the case of SKA in Ref. [102].

## C. Results

In this section we present the results of our forecast analysis. We compute  $1\sigma$  and  $2\sigma$  error ellipses for the parameters  $\Omega_{cdm} h^2$ ,  $10^9 A_s$ ,  $n_s$  and  $w_0$  in the different scenarios and marginalize over all the remaining parameters. Additionally we present histograms for the dark energy equation-of-state today and the spectral tilt.

In Fig. 5 we compare the HD model to a standard  $\Lambda$ CDM scenario. This comparison allows us to determine how well future data will be able to discriminate between two competing models that are currently close in parameter space and have a similar statistical significance. As argued in Section IIIC, for present cosmological data the HD parameter space is just a restriction of the  $\Lambda$ CDM one. Note, however, that in the HD scenario the spec-

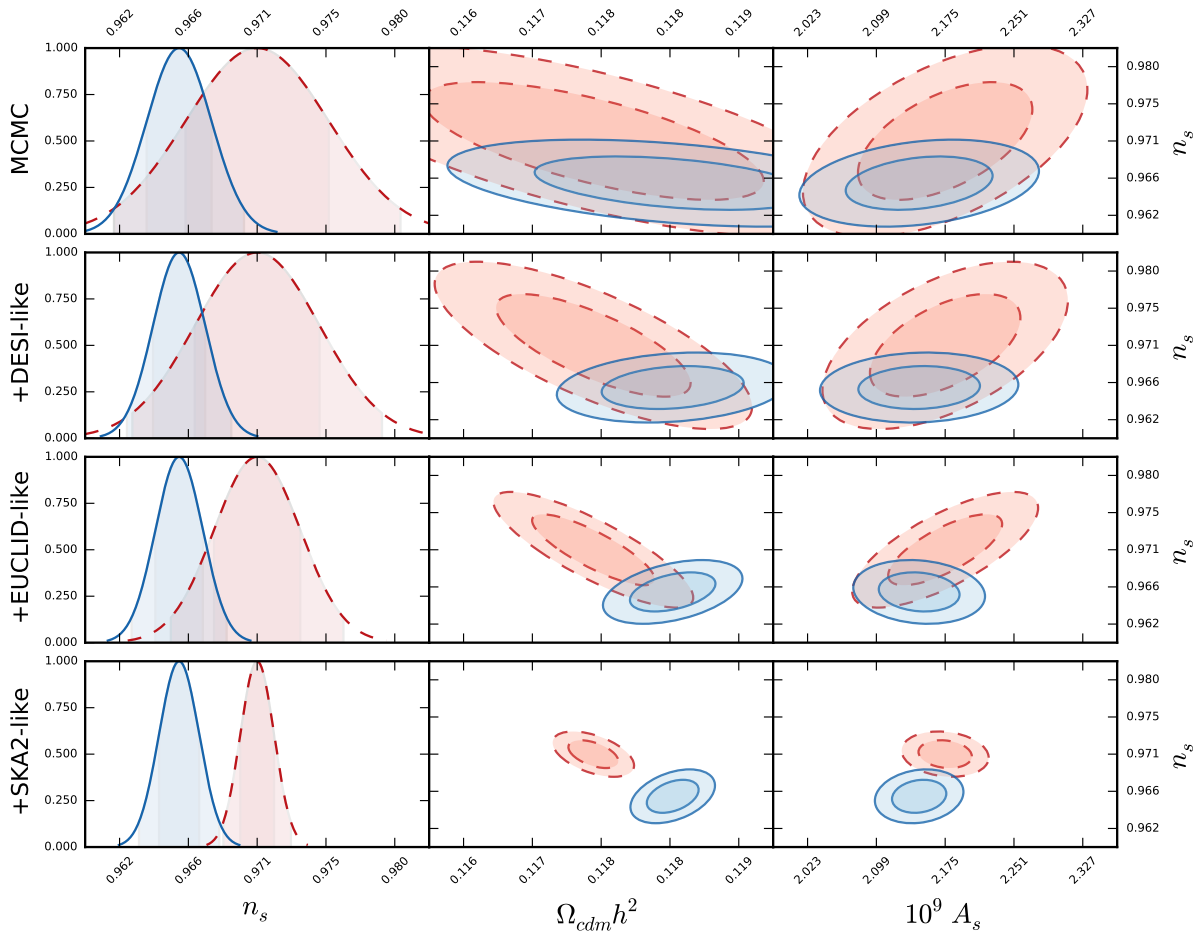


FIG. 5. Comparison of a  $\Lambda$ CDM (red, dashed) and a HD cosmology (blue, solid). The leftmost column shows the fully marginalized 1D Gaussian probability distribution for the  $n_s$  parameter. The second and third columns show the  $1\sigma$  and  $2\sigma$  2D Gaussian error contours. Each model is centered on the fiducial values obtained from *its own* MCMC run. We plot i) the constraints from the MCMC run in a Fisher approximation, and add to this ii) the constraints for a DESI-like mission considering GC on linear scales only iii) the constraints for a Euclid-like mission, combining GC on linear scales and WL non-linear and iv) the combination of constraints for an SKA2-like survey, with both GC and WL non-linear. All remaining parameters are marginalized over. A HD cosmology can be ruled out by a future measurement of large spectral tilt.

tral tilt is bounded from above for a theoretically well-motivated number of  $e$ -folds. In particular, for the mean value  $N_* = 60.7$ , we have  $n_s \lesssim 0.967$ , cf. Eq. (32). This is a first prediction of the HD model that sets it apart from the standard cosmological scenario. The upper bound on  $n_s$  has some interesting consequences for the outcome of future cosmological surveys. Indeed, if the preferred value for  $n_s$  moves to larger values in the future, even a pure GC DESI-like probe will be able to find clear differences between a HD cosmology and a  $\Lambda$ CDM one. If the current mean values for these two models are maintained in the presence of new data sets a combination of a Euclid-like or SKA2-like probe with present datasets translates into a  $\Lambda$ CDM value of  $n_s$  which is more than  $3\sigma$  away from the HD one, when analyzed from the point of view of a HD cosmology. A Bayesian inference approach will potentially be able to discriminate between these two

well-separated cases. In Table IV we list the estimated errors on the interesting parameters for a Euclid-like probe plus current cosmological data. This shows that the constraints on  $n_s$  will improve by a factor 2 in HD cosmology, mostly due to the effect of the consistency relations.

The results presented in Fig. 6 allow to estimate the constraining power of the consistency relations. In this figure, we display the error contours for the HD scenario and for a  $w$ CDM cosmology *centered at the HD central values* in order to facilitate the comparison. For present data sets, the error contours in the HD model are well inside the  $w$ CDM contours, showing that the constraining power of Planck data on the spectral tilt is enough to restrain the HD model in a way far beyond the limits of a model without consistency relations. The HD model is capable of predicting the complete background evolution of the Universe and therefore a precise

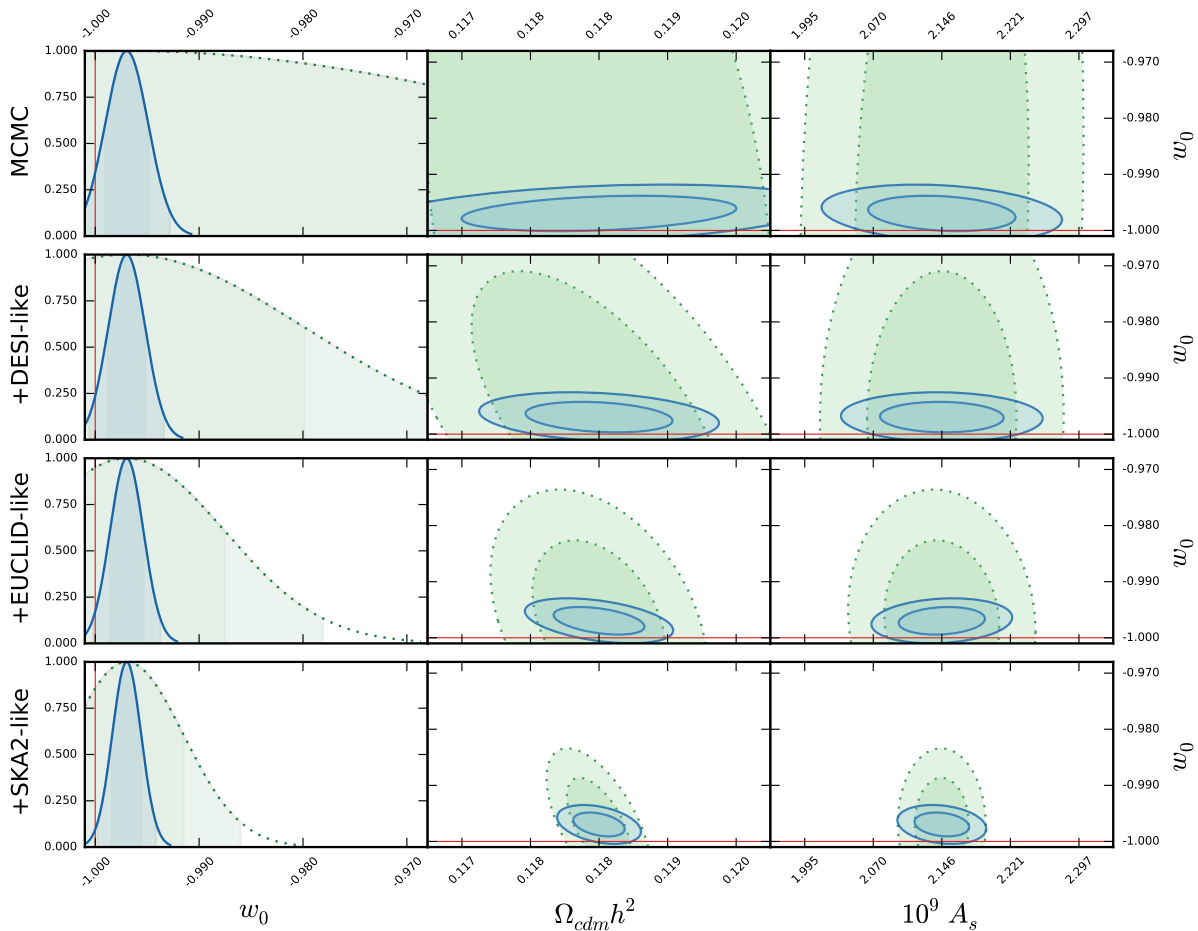


FIG. 6. Comparison of a HD cosmology (blue, solid) and a  $w$ CDM model (green, dotted) for the same observables and data as in Fig. 5. Note that the  $w$ CDM case is centered on the *Higgs-Dilaton fiducial values* (for example the MCMC mean value for  $w_0$  in  $w$ CDM is  $w_0 = -0.939 \pm 0.061$ ) to facilitate the comparison with the HD cosmology and to illustrate the impact of the consistency relations on parameter uncertainties, especially on the estimation of the present dark-energy equation-of-state parameter  $w_0$ . A HD cosmology can be ruled out by a measurement of a large  $w_0$  or if phantom dark energy is preferred by future data. For a futuristic SKA2-like survey, the cosmological constant scenario could be ruled out at the  $2\sigma$  level.

value for the dark energy equation-of-state parameter. This is a second clear prediction that is easy to test with future observations. Indeed, when analyzed with present data, the  $w$ CDM model provides a mean value  $w_0 = -0.939 \pm 0.061$ . If future data would favor this value of the dark energy equation of state, the HD scenario would be strongly disfavored. To accommodate a value  $w_0 \gtrsim -0.98$  and at the same time agree with measurements of  $n_s$ , one would need a number of  $e$ -folds of inflation in strong tension with theoretical estimates. In the same way, a measurement of a dark-energy equation-of-state parameter very close to that of a cosmological constant will also disfavor the HD model by roughly  $2\sigma$  in the more futuristic case.

The error contours in Figs. 5 and 6 also illustrate how the constraints on standard parameters get affected by the consistency relations. For instance, in Fig. 5 one can observe that the degeneracy direction between  $\Omega_{cdm}h^2$

and  $n_s$  as well as the degeneracy directions between  $10^9 A_s$  and  $n_s$  are rotated in the HD model (blue solid ellipses) as compared to the  $\Lambda$ CDM case (red dashed ellipses). This can be understood in terms of the correlation coefficients of the corresponding covariance matrices, see Fig. 7. Due to the strong correlation of  $n_s$  and  $w_0$  with  $N_*$ , of the order of  $+1$  and  $-1$  respectively, other correlations present in standard cosmology – for example the negative correlation between  $\Omega_{cdm}$  and  $n_s$  and the positive correlation between  $h$  and  $w_0$  – get sufficiently altered, such that in the HD cosmology one observes a positive correlation between  $n_s$  and  $\Omega_{cdm}$ . This breaks degeneracies in parameter space and helps to better constrain other cosmological parameters, although only slightly for the case of  $\Omega_{cdm}h^2$  and  $10^9 A_s$ , cf. Table IV.

The most important feature of the HD model is that it singles out a curve in the parameter space spanned by  $w_0, r, n_s, \alpha_s$ . A precise measurement of two or more of

	$\Lambda$ CDM	HD	$w$ CDM
$\Omega_{cdm}h^2$	0.40%	0.28%	0.43%
$10^9 A_s$	1.9%	1.4%	1.9%
$n_s$	0.29%	0.16%	0.31%
$w_0$	-	0.16%	0.95%

TABLE IV.  $1\sigma$  constraints from a Euclid-like probe combined with the MCMC covariance matrices obtained from present data, for the different models considered in this work. The constraining power of the consistency relations manifest as a reduction of the error on  $n_s$  by a factor 2 and on a reduction of the error on  $w_0$  by a factor 6 in the HD scenario. For the DESI-like survey we find the same trend, but with all relative errors roughly 50 % larger, while for the SKA2-like observation, the constraints improve roughly by a factor 2, consistent with the elliptical contours in Figs. 5 and 6.

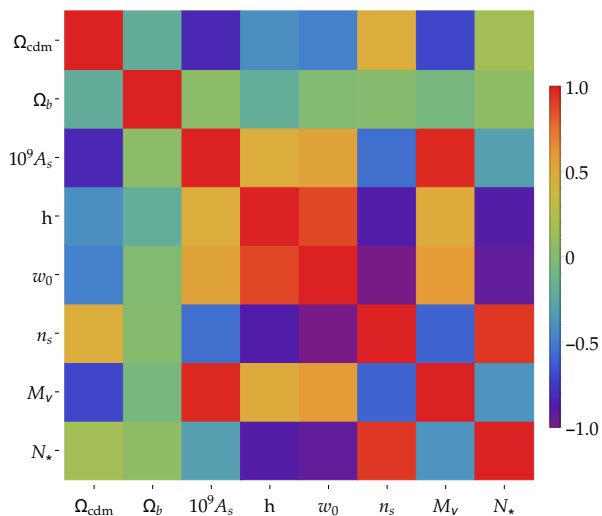


FIG. 7. Correlation matrix for the HD model forecast for a Euclid-like probe. The +1 and -1 limits stand respectively for *totally correlated* and *totally anticorrelated*.

these parameters provides a consistency check of the HD model. If the parameters inferred from data assuming a model different from HD cosmology do not fall onto the HD curve, the HD model will be challenged, and eventually the Bayesian evidence would favor other models.

We finish this section with a disclaimer. Although the Fisher Matrix technique allows for a quick estimate of the constraining power of future surveys, it is rooted on the assumption of a Gaussian approximation for the likelihood, which certainly fails for sharp restrictions such as the absence of negative neutrino masses or the absence of phantom behavior with  $w_0 < -1$  assumed in this paper. For this reason, it would be convenient to eventually perform a more robust forecast by sampling the observational likelihoods via an MCMC approach, which, in our case, should reflect the consistency relations our model imposes on the parameter space. In the context of this

analysis it would also be interesting to account for the effect of the non-flat priors suggested in Ref. [103]. These could potentially lead to mean values of  $w_0$  in the HD case even further away from  $w_0 = -1$ .

## V. CONCLUSION

The Higgs-Dilaton model is a scale-invariant extension of the Standard Model non-minimally coupled to unimodular gravity and containing just an additional degree of freedom on top of the Standard Model particle content. This minimalistic framework allows for a successful inflationary stage followed by a standard hot Big Bang era and a late-time dark-energy domination period. The inflationary and dark energy dominated eras turn out to be strongly related in the Higgs-Dilaton scenario. In particular, the model predicts a set of measurable consistency relations between the inflationary observables and the dark-energy equation-of-state parameter. We presented an alternative derivation of these consistency relations that highlights the connections and differences with  $\alpha$ -attractor scenarios [21–23] and allows for a straightforward generalization to the general scale-invariant scenarios considered in Ref. [49]. We studied the impact of the Higgs-Dilaton consistency relations on the analysis of present data sets and on the results of future galaxy surveys. To this end, we compared the Higgs-Dilaton model to a standard  $\Lambda$ CDM cosmology and to a  $w$ CDM scenario mimicking the dark-energy evolution of the Higgs-Dilaton model but without any additional constraints on the primordial power spectra. In the light of present data sets our results show that the Higgs-Dilaton model is preferred with respect to  $w$ CDM but still statistically indistinguishable from a  $\Lambda$ CDM cosmology. To estimate the discriminating power of future galaxy surveys, we used a Fisher Matrix approach to perform a forecast for the different scenarios, both for galaxy clustering and weak lensing probes. Assuming that the best fit values in these models remain comparable to the present values, we showed that both Euclid- and SKA2-like missions will be able to discriminate a Higgs-Dilaton cosmology from  $\Lambda$ CDM and  $w$ CDM. In particular, the Higgs-Dilaton model singles out a curve in the multiparameter space spanned by the spectral tilt of curvature perturbations, its running, the tensor-to-scalar ratio and the dark-energy equation-of-state parameter. A precise measurement of two or more of these parameters will provide a check of the HD model. On top of that, the strong correlation among them breaks degeneracies in parameter space by modifying other parameters' correlations without significantly altering their mean value with respect to  $\Lambda$ CDM.

## ACKNOWLEDGMENTS

We acknowledge support from the DFG through the project TRR33 “The Dark Universe”. MP acknowledges

support by the state of Baden-Württemberg through bwHPC.

- 
- [1] C. Wetterich, Nucl. Phys. **B302**, 668 (1988), arXiv:1711.03844 [hep-th].
- [2] C. Wetterich, Nucl. Phys. **B302**, 645 (1988).
- [3] C. Wetterich, Astron. Astrophys. **301**, 321 (1995), arXiv:hep-th/9408025 [hep-th].
- [4] K. A. Meissner and H. Nicolai, Phys. Lett. **B648**, 312 (2007), arXiv:hep-th/0612165 [hep-th].
- [5] M. Shaposhnikov and D. Zenhausern, Phys. Lett. **B671**, 187 (2009), arXiv:0809.3395 [hep-th].
- [6] J. Garcia-Bellido, J. Rubio, M. Shaposhnikov, and D. Zenhausern, Phys. Rev. **D84**, 123504 (2011), arXiv:1107.2163 [hep-ph].
- [7] D. Blas, M. Shaposhnikov, and D. Zenhausern, Phys. Rev. **D84**, 044001 (2011), arXiv:1104.1392 [hep-th].
- [8] F. Bezrukov, G. K. Karananas, J. Rubio, and M. Shaposhnikov, Phys. Rev. **D87**, 096001 (2013), arXiv:1212.4148 [hep-ph].
- [9] V. V. Khoze, JHEP **11**, 215 (2013), arXiv:1308.6338 [hep-ph].
- [10] K. Kannike, G. Hütsi, L. Pizza, A. Racioppi, M. Raidal, A. Salvio, and A. Strumia, JHEP **05**, 065 (2015), arXiv:1502.01334 [astro-ph.CO].
- [11] P. G. Ferreira, C. T. Hill, and G. G. Ross, Phys. Lett. **B763**, 174 (2016), arXiv:1603.05983 [hep-th].
- [12] P. G. Ferreira, C. T. Hill, and G. G. Ross, Phys. Rev. **D95**, 043507 (2017), arXiv:1610.09243 [hep-th].
- [13] K. Kannike, M. Raidal, C. Spethmann, and H. Veermäe, JHEP **04**, 026 (2017), arXiv:1610.06571 [hep-ph].
- [14] A. Shkerin, JHEP **05**, 155 (2017), arXiv:1701.02224 [hep-ph].
- [15] J. Rubio and C. Wetterich, Phys. Rev. **D96**, 063509 (2017), arXiv:1705.00552 [gr-qc].
- [16] W. A. Bardeen, in *Ontake Summer Institute on Particle Physics Ontake Mountain, Japan, August 27-September 2, 1995* (1995).
- [17] M. Shaposhnikov and D. Zenhausern, Phys. Lett. **B671**, 162 (2009), arXiv:0809.3406 [hep-th].
- [18] G. Marques Tavares, M. Schmaltz, and W. Skiba, Phys. Rev. **D89**, 015009 (2014), arXiv:1308.0025 [hep-ph].
- [19] G. K. Karananas and M. Shaposhnikov, Phys. Rev. **D93**, 084052 (2016), arXiv:1603.01274 [hep-th].
- [20] G. K. Karananas and M. Shaposhnikov, (2017), arXiv:1708.02220 [hep-th].
- [21] S. Ferrara, R. Kallosh, A. Linde, and M. Porrati, Phys. Rev. **D88**, 085038 (2013), arXiv:1307.7696 [hep-th].
- [22] R. Kallosh, A. Linde, and D. Roest, JHEP **11**, 198 (2013), arXiv:1311.0472 [hep-th].
- [23] M. Galante, R. Kallosh, A. Linde, and D. Roest, Phys. Rev. Lett. **114**, 141302 (2015), arXiv:1412.3797 [hep-th].
- [24] DESI Collaboration, A. Aghamousa, and others, arXiv:1611.00036 [astro-ph] (2016).
- [25] DESI Collaboration, A. Aghamousa, and others, arXiv:1611.00037 [astro-ph] (2016).
- [26] L. Amendola and others, Living Reviews in Relativity **16** (2013), 10.12942/lrr-2013-6.
- [27] R. Laureijs and others, arXiv:1110.3193 [astro-ph] (2011).
- [28] S. Yahya, P. Bull, M. G. Santos, M. Silva, R. Maartens, P. Okouma, and B. Bassett, Monthly Notices of the Royal Astronomical Society **450**, 2251 (2015).
- [29] M. G. Santos, D. Alonso, P. Bull, M. Silva, and S. Yahya, arXiv:1501.03990 [astro-ph] (2015).
- [30] A. Raccanelli, P. Bull, S. Camera, D. Bacon, C. Blake, O. Dore, P. Ferreira, R. Maartens, M. Santos, M. Viel, and G.-b. Zhao, (2015).
- [31] P. Bull, S. Camera, A. Raccanelli, C. Blake, P. G. Ferreira, M. G. Santos, and D. J. Schwarz, arXiv:1501.04088 [astro-ph] (2015).
- [32] B. Allen and A. Folacci, Phys. Rev. **D35**, 3771 (1987).
- [33] J. Jalmuzna, A. Rostworowski, and P. Bizon, Phys. Rev. **D84**, 085021 (2011), arXiv:1108.4539 [gr-qc].
- [34] I. Antoniadis, J. Iliopoulos, and T. N. Tomaras, Phys. Rev. Lett. **56**, 1319 (1986).
- [35] N. C. Tsamis and R. P. Woodard, Phys. Lett. **B301**, 351 (1993).
- [36] N. C. Tsamis and R. P. Woodard, Annals Phys. **238**, 1 (1995).
- [37] I. Antoniadis, P. O. Mazur, and E. Mottola, New J. Phys. **9**, 11 (2007), arXiv:gr-qc/0612068 [gr-qc].
- [38] A. M. Polyakov, Nucl. Phys. **B834**, 316 (2010), arXiv:0912.5503 [hep-th].
- [39] C. Wetterich, Phys. Lett. **B773**, 6 (2017), arXiv:1704.08040 [gr-qc].
- [40] J. J. van der Bij, H. van Dam, and Y. J. Ng, Physica **116A**, 307 (1982).
- [41] F. Wilczek, *Nuffield Workshop on the Very Early Universe Cambridge, England, June 21-July 9, 1982*, Phys. Rept. **104**, 143 (1984).
- [42] W. Buchmuller and N. Dragon, Phys. Lett. **B207**, 292 (1988).
- [43] W. G. Unruh, Phys. Rev. **D40**, 1048 (1989).
- [44] S. Weinberg, Rev. Mod. Phys. **61**, 1 (1989).
- [45] M. Henneaux and C. Teitelboim, Phys. Lett. **B222**, 195 (1989).
- [46] W. Buchmuller and N. Dragon, Phys. Lett. **B223**, 313 (1989).
- [47] Yu. F. Pirogov, in *14th International Seminar on High Energy Physics: Quarks 2006 St. Petersburg, Russia, May 19-25, 2006* (2006) arXiv:gr-qc/0609103 [gr-qc].
- [48] E. Alvarez, D. Blas, J. Garriga, and E. Verdaguer, Nucl. Phys. **B756**, 148 (2006), arXiv:hep-th/0606019 [hep-th].
- [49] G. K. Karananas and J. Rubio, Phys. Lett. **B761**, 223 (2016), arXiv:1606.08848 [hep-ph].
- [50] F. Bezrukov, D. Gorbunov, and M. Shaposhnikov, JCAP **0906**, 029 (2009), arXiv:0812.3622 [hep-ph].
- [51] J. Garcia-Bellido, D. G. Figueroa, and J. Rubio, Phys. Rev. **D79**, 063531 (2009), arXiv:0812.4624 [hep-ph].

- [52] F. Bezrukov, D. Gorbunov, and M. Shaposhnikov, *JCAP* **1110**, 001 (2011), arXiv:1106.5019 [hep-ph].
- [53] B. Ratra and P. J. E. Peebles, *Phys. Rev.* **D37**, 3406 (1988).
- [54] P. G. Ferreira and M. Joyce, *Phys. Rev.* **D58**, 023503 (1998), arXiv:astro-ph/9711102 [astro-ph].
- [55] R. R. Caldwell and E. V. Linder, *Phys. Rev. Lett.* **95**, 141301 (2005), arXiv:astro-ph/0505494 [astro-ph].
- [56] V. F. Mukhanov, H. A. Feldman, and R. H. Brandenberger, *Phys. Rept.* **215**, 203 (1992).
- [57] M. Artymowski and J. Rubio, *Phys. Lett.* **B761**, 111 (2016), arXiv:1607.00398 [astro-ph.CO].
- [58] T. Terada, *Phys. Lett.* **B760**, 674 (2016), arXiv:1602.07867 [hep-th].
- [59] J. Garcia-Bellido, J. Rubio, and M. Shaposhnikov, *Phys. Lett.* **B718**, 507 (2012), arXiv:1209.2119 [hep-ph].
- [60] J. Repond and J. Rubio, *JCAP* **1607**, 043 (2016), arXiv:1604.08238 [astro-ph.CO].
- [61] F. Bezrukov, J. Rubio, and M. Shaposhnikov, *Phys. Rev.* **D92**, 083512 (2015), arXiv:1412.3811 [hep-ph].
- [62] J. Rubio and M. Shaposhnikov, *Phys. Rev.* **D90**, 027307 (2014), arXiv:1406.5182 [hep-ph].
- [63] C. Wetterich, in *Proceedings, 5th International Conference on Strong and Electroweak Matter (SEWM 2002): Heidelberg, Germany, October 2-5, 2002* (2003) pp. 230–249, arXiv:hep-ph/0302116 [hep-ph].
- [64] R. J. Scherrer and A. A. Sen, *Phys. Rev.* **D77**, 083515 (2008), arXiv:0712.3450 [astro-ph].
- [65] T. Chiba, A. De Felice, and S. Tsujikawa, *Phys. Rev.* **D87**, 083505 (2013), arXiv:1210.3859 [astro-ph.CO].
- [66] E. J. Copeland, A. R. Liddle, and D. Wands, *Phys. Rev.* **D57**, 4686 (1998), arXiv:gr-qc/9711068 [gr-qc].
- [67] F. Bezrukov, M. Yu. Kalmykov, B. A. Kniehl, and M. Shaposhnikov, *Helmholtz Alliance Linear Collider Forum: Proceedings of the Workshops Hamburg, Munich, Hamburg 2010-2012, Germany*, *JHEP* **10**, 140 (2012), [275(2012)], arXiv:1205.2893 [hep-ph].
- [68] G. Degrassi, S. Di Vita, J. Elias-Miro, J. R. Espinosa, G. F. Giudice, G. Isidori, and A. Strumia, *JHEP* **08**, 098 (2012), arXiv:1205.6497 [hep-ph].
- [69] D. Buttazzo, G. Degrassi, P. P. Giardino, G. F. Giudice, F. Sala, A. Salvio, and A. Strumia, *JHEP* **12**, 089 (2013), arXiv:1307.3536 [hep-ph].
- [70] F. Bezrukov and M. Shaposhnikov, *J. Exp. Theor. Phys.* **120**, 335 (2015), [*Zh. Eksp. Teor. Fiz.*147,389(2015)], arXiv:1411.1923 [hep-ph].
- [71] R. Armillis, A. Monin, and M. Shaposhnikov, *JHEP* **10**, 030 (2013), arXiv:1302.5619 [hep-th].
- [72] F. Gretschnig and A. Monin, *Phys. Rev.* **D92**, 045036 (2015), arXiv:1308.3863 [hep-th].
- [73] M. E. Shaposhnikov and F. V. Tkachov, (2009), arXiv:0905.4857 [hep-th].
- [74] F. Bezrukov and M. Shaposhnikov, *Phys. Lett.* **B734**, 249 (2014), arXiv:1403.6078 [hep-ph].
- [75] Y. Hamada, H. Kawai, K.-y. Oda, and S. C. Park, *Phys. Rev. Lett.* **112**, 241301 (2014), arXiv:1403.5043 [hep-ph].
- [76] F. Bezrukov, M. Pauly, and J. Rubio, (2017), arXiv:1706.05007 [hep-ph].
- [77] B. Audren, J. Lesgourgues, K. Benabed, and S. Prunet, *JCAP* **1302**, 001 (2013), arXiv:1210.7183 [astro-ph.CO].
- [78] D. Blas, J. Lesgourgues, and T. Tram, *JCAP* **1107**, 034 (2011), arXiv:1104.2933 [astro-ph.CO].
- [79] N. Aghanim *et al.* (Planck), *Astron. Astrophys.* **594**, A11 (2016), arXiv:1507.02704 [astro-ph.CO].
- [80] P. A. R. Ade *et al.* (BICEP2, Keck Array), *Phys. Rev. Lett.* **116**, 031302 (2016), arXiv:1510.09217 [astro-ph.CO].
- [81] M. Betoule *et al.* (SDSS), *Astron. Astrophys.* **568**, A22 (2014), arXiv:1401.4064 [astro-ph.CO].
- [82] F. Beutler, C. Blake, M. Colless, D. H. Jones, L. Staveley-Smith, L. Campbell, Q. Parker, W. Saunders, and F. Watson, *Mon. Not. Roy. Astron. Soc.* **416**, 3017 (2011), arXiv:1106.3366 [astro-ph.CO].
- [83] L. Anderson *et al.* (BOSS), *Mon. Not. Roy. Astron. Soc.* **441**, 24 (2014), arXiv:1312.4877 [astro-ph.CO].
- [84] A. J. Ross, L. Samushia, C. Howlett, W. J. Percival, A. Burden, and M. Manera, *Mon. Not. Roy. Astron. Soc.* **449**, 835 (2015), arXiv:1409.3242 [astro-ph.CO].
- [85] M. Trushorras, S. Nesseris, and J. Garcia-Bellido, *Phys. Rev.* **D94**, 063511 (2016), arXiv:1604.06760 [astro-ph.CO].
- [86] R. E. Kass and A. E. Raftery, *Journal of the American Statistical Association* **90**, 773 (1995).
- [87] A. Heavens, Y. Fantaye, A. Mootoivaloo, H. Eggers, Z. Hosenie, S. Kroon, and E. Sellentin, (2017), arXiv:1704.03472 [stat.CO].
- [88] A. Heavens, Y. Fantaye, E. Sellentin, H. Eggers, Z. Hosenie, S. Kroon, and A. Mootoivaloo, *Phys. Rev. Lett.* **119**, 101301 (2017), arXiv:1704.03467 [astro-ph.CO].
- [89] M. Levi, C. Bebek, T. Beers, R. Blum, R. Cahn, D. Eisenstein, B. Flaugher, K. Honscheid, R. Kron, O. Lahav, P. McDonald, N. Roe, D. Schlegel, and r. t. D. collaboration, arXiv:1308.0847 [astro-ph] (2013).
- [90] S. Casas, M. Kunz, M. Martinelli, and V. Pettorino, *Physics of the Dark Universe* **18**, 73 (2017).
- [91] L. Amendola *et al.*, (2016), arXiv:1606.00180 [astro-ph.CO].
- [92] I. Harrison, S. Camera, J. Zuntz, and M. L. Brown, arXiv:1601.03947 [astro-ph] (2016).
- [93] M. Tegmark, A. Hamilton, M. Strauss, M. Vogeley, and A. Szalay, *The Astrophysical Journal* **499**, 555 (1998).
- [94] H.-J. Seo and D. J. Eisenstein, *The Astrophysical Journal* **665**, 14 (2007).
- [95] H.-J. Seo and D. J. Eisenstein, *The Astrophysical Journal* **633**, 575 (2005).
- [96] P. Bull, arXiv:1509.07562 [astro-ph, physics:gr-qc] (2015).
- [97] S. de la Torre and L. Guzzo, arXiv:1202.5559 [astro-ph] (2012).
- [98] L. Amendola, V. Pettorino, C. Quercellini, and A. Vollmer, *Physical Review D* **85** (2012), 10.1103/PhysRevD.85.103008.
- [99] M. Bartelmann and P. Schneider, *Phys. Rept.* **340**, 291 (2001), arXiv:astro-ph/9912508 [astro-ph].
- [100] R. Takahashi, M. Sato, T. Nishimichi, A. Taruya, and M. Oguri, *Astrophys. J.* **761**, 152 (2012), arXiv:1208.2701 [astro-ph.CO].
- [101] S. Bird, M. Viel, and M. G. Haehnelt, *Mon. Not. Roy. Astron. Soc.* **420**, 2551 (2012), arXiv:1109.4416 [astro-ph.CO].
- [102] D. Kirk, A. Benoit-Lévy, F. B. Abdalla, P. Bull, and B. Joachimi, (2015), arXiv:1501.03848 [astro-ph.CO].
- [103] S. Hannestad and T. Tram, (2017), arXiv:1710.08899 [astro-ph.CO].